

To be submitted to Building and Environment, 2022

Assessment of exhaled pathogenic droplet dispersion and indoor-outdoor exposure risk in urban street with naturally-ventilated buildings

Jian Hang[1], Xia Yang[2,3#], Cuiyun Ou[1#], Zhiwen Luo[4], Xiaodan Fan[1], Xuelin Zhang[1], Zhongli Gu[5], Xianxiang Li[1*]

[1]School of Atmospheric Sciences, Sun Yat-sen University, Southern Marine Science and Engineering Guangdong Laboratory (Zhuhai), Zhuhai, P.R. China

[2]Guangdong Province Engineering Laboratory for Air Pollution Control, Guangzhou, P.R. China

[3]Guangdong Provincial Key Laboratory of Water and Air Pollution Control, Guangzhou, P.R. China

[4] Welsh School of Architecture, Cardiff University, UK

[5] Guangdong Fans-tech Agro Co., Ltd. China

[#]These authors contribute equally as the first author (Jian Hang, Xia Yang, Cuiyun Ou).

Corresponding author: Xianxiang Li

Email: lixx98@mail.sysu.edu.cn

Abstract

Outdoor droplet exposure risk is generally regarded much smaller than that indoor, but such indoor-outdoor assessment and comparison are still rare. By coupling indoor and outdoor environments, we numerically simulate the ventilation and dispersion of exhaled pathogenic droplets (e.g., diameter d=10μm) within typical street canyon (outdoor, aspect ratio H/W=1) and each room (indoor) of two eight-floor single-sided naturally-ventilated buildings. Inhaled fraction (*IF*) and suspended fraction (*SF*) between two face-to-face people are calculated to quantify and compare the human-to-human exposure risk in all 16 rooms (indoor) on eight floors and those at two outdoor sites. Numerical simulations are validated well by wind tunnel experiments.

Results show that, the rooms in the 1st and 8th floors attain greater air change rate per hour (~4.5-6.6h^{-1}) and the lower exposure risk (*IF*~2-4ppm) than the 2nd-7th floors (air change rate per hour~1.6-5.3h^{-1}, *IF*~4-11ppm). Although inter-floor droplet dispersion exists, the room with index patient attains 2-4 order greater exposure risk than the other rooms without index patient. When the index patient stays outdoor, outdoor *IF* will change with locations, i.e. ~55ppm at leeward corner (even exceeding indoor *IF*~2-11ppm), and ~7ppm at middle street. Hence, the outdoor infection risk should not be ignored especially for people at leeward street corner where small vortex exists inducing local weak ventilation. Particularly, outdoor *IF* is decided by short-distance spraying droplet exposure (~1m) and long-route airborne transmissions by the main recirculation through entire street canyon (~50-100m).

Key Words: street canyon, air change rate per hour (*ACH*), indoor and outdoor, droplet

dispersion, exposure risk

Environmental implication

Respiratory infectious diseases can spread indoor and outdoor by exhaled droplets carrying pathogenic bacteria/viruses. Most researches emphasize indoor exposure risk (e.g. isolation room, airplane cabins, restaurants, coach buses etc). However, outdoor exposure risk assessments are still rare. The comparison of infection risks between indoor and outdoor environments also requires further investigations.

We innovatively simulate/discuss the ventilation and exhaled pathogenic droplets dispersion(10μm) in rooms of 8-floor naturally-ventilated buildings (indoor) and street canyons (outdoor). Inhaled fraction (*IF*) is calculated to evaluate human-to-human exposure risk. Results indicate that indoor *IF* are 2-11ppm, but outdoor *IF* varies with locations, i.e. ~55ppm in leeward corner (exceeding indoor *IF*), ~7ppm at middle street.

1 Introduction

Respiratory infectious diseases, such as SARS in 2003, global influenza in 2009, the Middle East Respiratory Syndrome (MERS) in 2012, and COVID-19 in 2019-2022, have been indicated to spread rapidly among people by pathogen-laden droplet transmissions [1], which seriously threatens public health. Currently, there are more than 610 million confirmed COVID-19 cases worldwide, including over 6 million deaths [2]. Therefore, it has become an important scientific issue to study the pathogen-laden droplet dispersion and human-to-human exposure risks.

Numerous experiments and numerical simulations have been developed to study the mechanisms of droplet transmission in various indoor environments, including hospital isolation rooms [3-5], airplane cabins [6-8], coach buses [9-11]), within and between naturally-ventilated buildings with cross-corridor transmission and that between flats [12, 13]. Tung et al. [14] experimentally investigated contaminant dispersion in an isolation room with different ventilation rates and negative pressure differentials. Based on the experimental studies [15], Gupta et al. [6] found that airborne transmission of respiratory infectious diseases could occur in an aircraft cabin. Cheng et al. [12] investigated the cross-corridor transmission of SARS-CoV-2 due to cross airflows, suggesting a high exposure risk at downstream flats under a prevailing wind, with higher risk when the doors or windows connected to the corridor were open. These findings suggest that the exposure risk of airborne transmission is influenced significantly by ventilation airflow patterns in indoor environment. Moreover, the indoor ventilation airflow pattern is mainly controlled by the supply air and relative positions of the inlet and outlet, since the ambient wind speed is relatively less important. Besides, Ventilation pattern, buoyancy force induced by thermal bodies produces significant upward airflow (~0.1m/s), significantly impact on indoor airflow patterns [16, 17]. Airborne transmission and infection risk between flats and different floors are assessed for residential building models with wind-driven ventilation [18], buoyancy-driven ventilation [13] and for street canyons by coupling indoor and outdoor [19]. But they did not compare the infection risk between flats and that in local rooms with index patient.

For outdoor places, most previous researches emphasized the dispersion of inert or reactive gaseous pollutants and particles as well as pollutant exposure in urban environments [20-25], but few investigate the dispersion of exhaled droplets from human breathing activities in outdoor urban space which may evaporate and is a kind of hazardous material carrying infectious bacterial or viruses. In recent years, limited researches explore droplet evaporation/dispersion in an outdoor open space [26-27] and a street canyon [28]. They found that human-to-human infection risks outdoor cannot be neglected when the index patient locates in the upstream regions of other people.. However, there are occasional reports of outdoor infection, which suggests a probable of outdoor airborne transmission. Blocken et al. [26] have indicated the influence of wind speed on the outdoor social distance between two moving pedestrians by posing different levels of airborne infection risk. Yang et al. [27] have numerically investigated the transmission of solid-liquid droplets between two standing people in an open outdoor environment. They suggested that people in outdoors should not only keep a more than 1.5 m social distance from each other, but also avoid standing in the downstream region of infected persons. Fan et al. [28] have numerically simulated the interpersonal droplet transmission between two people in a two-dimensional street canyon (*H/W*=2.4). They suggested a 2 m social distance for pedestrians in deep urban street canyons with high winds, while 4 m with low wind speed (*WS*) and small relative humidity (*RH*). Hence, the outdoor transient environmental conditions, such as *WS*, temperature and *RH*, are important to determine the airborne transmission risk for outdoor places [29]. Among them, ventilation and buoyancy force respectively driven by wind and temperature differential are key to transport and dilute outdoor airborne droplets and droplets [30], which may penetrate to the nearby buildings with openings, and subsequently expose people there to airborne droplets, and vice versa [31].

However, there is rare research to compare and quantify exhaled droplet dispersion and the related human-to-human infection risk analysis in urban street canyon and ventilated buildings by coupling indoor and outdoor. Some questions are still not clear, for instance: 1) Is outdoor exposure risk is definitely smaller than indoor? What difference between them? 2) Exposure risk between flats and buildings has not been compared with that in the target room with index patient. 3) The exposure risk due to transmissions from outdoor to indoor is still unclear.

In addition, according to the literature, droplet initial size, ambient temperature and relative humidity, background wind speed are the key factors of droplet dispersion [16-17, 27-28, 32]. Here we considered the specific conditions where the affecting ambient environment parameters including air temperature (300 K), *RH* (35%), *WS* (3 m/s), and airflow pattern [11, 32-33]. The physical and chemical characteristics of droplets (e.g., the initial size (10μm), initial velocity, the droplet components, etc) were also considered as significant factors to affect the spread of respiratory infectious diseases [24, 34-35].

This study aims to address the gap in the literature about ventilation performance and droplet dispersion in the indoor and outdoor coupling street canyon model with naturally-ventilated buildings, which can simultaneously consider the droplet dispersion in outdoors (urban street canyon) and indoors (the nearby building rooms). In this study, we comprehensively assessed the droplet dispersion in urban street canyons, evaluating the possibility of airborne transmission among different room of multi-floor buildings, street canyons and those between them.

2 Methodology

2.1 CFD validation study

2.1.1. CFD validation and grid independent tests in street canyons

To evaluate the numerical accuracy of ventilation simulations in the 2-D street canyon, we compared the flow field of CFD simulations with the wind tunnel experiments in University of Gavle, Sweden [20]. The placements of wind tunnel experiments are displayed in Fig.1a. There are 25 rows of building models in the working section, which is 11 m long, 3 m wide, and 1.5 m high. Velocity profiles at Line A between the 12th and 13th buildings and Line B above the 12th building are measured to be used in the subsequent CFD computations.

The geometric dimension of the wind tunnel model is the building height H = 0.12 m, the street width is equal to the building width (W = B = 0.05 m), and the scale ratio to the full-size street canyon model is 1:200 (H = 24 m, W = B = 10 m, Fig. 1b). The approaching wind is perpendicular to the street array, with the reference velocity U_{ref} = 13 m/s at z = H in far upstream free flow. The corresponding Reynolds number (Re = $U_{ref}H/v$, v = 1.46×10^{-5} m^2/s) is 106,849, big enough to satisfy the Reynolds independence. In the present CFD simulation, zero normal gradient boundary conditions are adopted at the domain outlet (i.e., outflow), domain roof and lateral boundaries (i.e., symmetry). Fig.1c-d illustrate the stream-wise velocity (u(z)) components and turbulence kinetic energy (k(z)) along Line B, which is measured by Laser Doppler Anemometry (LDA) System to provide the domain inlet boundary under U_{ref} = 13 m/s.

Grid independent tests have been done by different minimum grid sizes near the building walls (Fig. 2), named as fine grid (0.05 m), medium grid (0.1 m) and coarse grid (0.2 m). And the expansion ratio is 1.0-1.2 which is smaller than 1.3 satisfying the requirement by the literature of CFD guideline [36-37]. It shows that there is tiny difference among the results of the three different grid arrangements. In order to ensure accuracy and save computational time, the medium grid will be adopted to evaluate the flow field in the following cases. High correlation coefficient (R~0.993), low normalized mean square error ($NMSE$~0.004) and low fractional bias (FB~0.017) have been found between experiments data and simulation results, which shows that the predicted stream-wise velocity ($u(z)$) profiles agree well with the measured data. The numerical simulation results also indicate that the stream-wise velocity is positive above z = 0.5H while negative below it. This confirms that one main vortex appears as H/W = 2.4 with sufficiently large Re (>> 11,000) [38-40].

The coupled approach means simultaneously simulating both indoor and outdoor environments in a single computational domain. Our previous research [41] has validated that the couple approach can perform well in evaluating the indoor and outdoor ventilation [36-37,42]. Hence, it can be reasonably applied in the following investigation.

2.1.2. Validation of building ventilation

Another measurement of indoor-outdoor airflow is also carried out in the aforementioned wind tunnel. A four-floor building with single-sided natural ventilation is located in the target measurement area (Fig.3a). Each floor is divided into two rooms by a partition in the middle, and the only window of each room is perpendicular to the incoming flow. Steam-wise (U_x) and vertical (U_z) velocity components profiles along Line PA and Line PB around the building are measured (Fig.3a) to evaluate the simulation performance of building ventilation.

In the following validation, we build a model according to the wind tunnel experiment (Fig.3b) with a scale ratio of 50:1 to wind tunnel models. The single-sided natural ventilation building is $5H$, $5H$, and $10H$ away from the domain inlet, lateral sides and domain outlet. For the domain inlet, the measured profiles of velocity (u) and turbulent parameters (turbulence kinetic energy (k) and its dissipation rate (ε)) are provided in the upstream free flow (Fig.3c-d).

Fig.4a-b compares wind tunnel data and CFD results in terms of the stream-wise and vertical velocity components along Line PA and Line PB. It indicates that simulation results can predict the flow before and behind the building. While the results also show that the simulation results in Line PB above the building deviate from the measurement data to some extent ($1 < z/H < 1.4$). Such phenomenon can be attributed to that the RNG k-ε model has some shortcomings in describing the airflow in the corner area [43]. However, on the whole view, the CFD simulation model validated above is a helpful tool in the following investigation.

2.2 CFD modelling setups

There are two ways in indoor-outdoor flow simulations, namely decoupled and coupled approaches [44-46]. The decoupled approach simulates the indoor and outdoor airflow separately in different computational domains. While, the coupled approach builds indoor and outdoor environments in a single domain, which has been applied in our study on the indoor-outdoor ventilation and droplet dispersion.

Fig. 5a depicts the simplified street canyon in CFD simulation. The building height (H) and the street width (W) are 24 m. The span-wise length (y-direction) of the street canyon (L) and the building width (B) are 20 m. A typical street canyon is displayed in the front and rear of the target building to serve as roughness elements in the urban boundary layer [17, 47-49]. There are eight floors, and each floor is 3 m high with a 0.3 m thick floor slab in the near-road building. The wall thickness is 0.3 m and the size of each room is 5.7 m×4 m×2.7 m (length × width × height). We considered the natural ventilation of single-sided buildings with an opening (1.5 m×1.5 m) in the wall of every windward or leeward room. In order to investigate the exposure risk of the susceptible person who stays in the same room with the infected, we set two face-to-face people in a single room, with one susceptible and the other infected. The distance between them is 1.5 m which is the recommended smallest safe distance in Liu et al. [50]. In most cities, there are pedestrian streets for people to walk and shop in, and these places seem to be prone to disease transmission events. Therefore, the following scenarios of people in outdoor environment are considered: two people stand symmetrically along the central plane (y = 0) of the street canyon, with a distance of 0.5 m away from the nearby building leeward and in the middle of the canyon. Detailed information of building and human model has been illustrated in Fig.5a-b.

Mesh information on the central plane and manikin is provided in Fig. 5c, where the grid size of the mouth is 0.005 m, and those of other parts of manikin are 0.05 m. The medium grid arrangement (0.1 m) with the expansion ratio of 1.05-1.15 is adopted near the building walls with the total grids of about 11 million. At the domain inlet, the vertical profiles of velocity ($U_x(z)$), turbulent kinetic energy ($k(z)$) and turbulent dissipation rate ($\varepsilon(z)$) are calculated as follows [51]:

$$U_{x}(z) = U_{ref}(\frac{z-H}{z_{ref}})^{0.22} \tag{1a}$$

$$k(z) = (U_x(z) \times I_{in})^2 \tag{1b}$$

$$\varepsilon(z) = \frac{C_\mu^{3/4} K^{3/2}}{k(z)} \tag{1c}$$

Where the reference velocity U_{ref} = 3 m/s. The building height H equals to the reference height z_{ref} which is 24 m in this study. The turbulence intensity $I_{in} = 0.1$. Von Karman constant K=0.41 and C_μ=0.09 are empirical constants. At the lateral, upper and outlet boundaries of the computational domain, the normal velocity component and normal gradients of tangential velocity components are set to zero, i.e., zero normal gradient. Background temperature is set to 300 K (26.85 ℃), and the heat flux of the body surface is 58 W/m^2 [3].

There are two groups of numerical settings on breathing activities in previous researches: i) In the first group, the droplets are released periodically during a period like unsteady/transient breathing, talking, coughing, speech [15, 33, 50] etc. ii) In the second group, some literature utilized the mean and constant expiration flow rate as exhale boundary, and the droplet dispersion is also released continuously [9, 10, 52].

This simplification can not only effectively predict the droplet dispersion characteristics but also efficiently mitigate the cost of computational resources. For simplification, this study considers the respiratory activity that the infected person only exhales and the susceptible person only inhales with the mass flow rate of 1.225×10^{-4}kg/s [11, 27].

The governing equations are discretized to algebraic on a staged grid system based on the finite volume method. SIMPLE algorithm is applied to couple pressure and velocity. Standard wall function has been used in near wall treatment. The convection and diffusion terms are discretized with second-order upwind scheme. Convergence is assumed to be obtained when residuals of *x*, *y* and *z* momentum are stably smaller than 10^{-6}, 10^{-5} for *k*, and 10^{-4} for ε and continuity [53].

In this study, droplets with the initial diameter of 10 μm are composed of 90% liquid (water) and 10% solid elements (sodium chloride) [54]. The density of water liquid and sodium chloride are 1000 kg·m^{-3} and 2170 kg·m^{-3} respectively and the droplet density follow the volume weighted mixing law. The Lagrangian method is adopted to solve the motion equation of a single droplet. According to Newton's second law, the equation of droplet movement can be written as Eq. (3):

$$\frac{\mathrm{d}u_{\mathrm{pi}}}{\mathrm{dt}} = \sum F_i = F_{drag,i} + F_{g,i} + F_{a,i} \tag{3a}$$

$$\begin{aligned} F_{drag,i} &= f_D\left(u_i - u_{p,i}\right)/\tau_p \\ &= 18\mu\left(u_i - u_{p,i}\right)\left(1 + 0.15{Re_p}^{0.687}\right)/\left(\rho_p d_p^2 C_c\right) \end{aligned} \tag{3b}$$

$$F_{g,i} = g_i\left(\rho_p - \rho\right)/\rho_p \tag{3c}$$

where $\mathrm{u_{pi}}$ and $\mathrm{u_i}$ are the droplet and the air velocity vector respectively (m/s), $\sum \mathrm{F_i}$ is all external forces exerted on the droplet per unit droplet mass (m/s^2) in the *i* direction. $\mathrm{F_{drag,i}}$, $\mathrm{F_{g,i}}$, $\mathrm{F_{a,i}}$ respectively represent the drag force, gravity and the additional forces on the droplet [55-56]. $\mathrm{f_D}$ is the Stoke's drag modification function for large aerosol Reynolds number (Re_p) and τ_p is the aerosol characteristic response time (s). ρ_p and ρ are the droplet and air density ($kg \cdot m^{-3}$). d_p is the droplet diameter (m) and μ is the turbulent viscosity ($kg \cdot m^{-1} \cdot s^{-1}$). C_c is the Cunningham correction to Stokes drag law. g_i is the acceleration of gravity in the *i* direction. $F_{a,i}$ is the additional forces consisting of the pressure force, virtual mass force, Brownian force, and Saffman's lift force. Among them, the pressure force and virtual mass force are sufficiently small for indoor and outdoor droplet dispersion and so they are ignored according to the literature [47,55,57], thus this paper only considered the Brownian force and Saffman's lift force.

The dispersion of droplets owing to turbulent flows was predicted using the discrete random walk model-DRM. In the computational domain, the interaction between particles and airstreams is calculated as one-way coupling (i.e. the influence of droplets themselves on turbulent airflow is negligible) to save computational load. Droplet boundary conditions are list in Table. 1, the droplet will be inhaled by the susceptible person (the person shaded with yellow in Fig.5a) who located at each floor and the canyon, e.g. those droplet escape from the domain through the human mouth. The building wall and human body surface are thought to be rough and the droplet will deposit on these surfaces. If the droplet be inhaled by human or be trapped by subject, their calculation of trajectories is terminated.

After the steady flow field was obtained, respiratory droplets have released from the direction perpendicular to the index patient mouth at a rate of 44 droplets per time step (0.01s for a time step) for 15 minutes, totaling 3,960,000 number of droplets. At this stage, the diffusion range remains stable, and the normalized constants—inhaled fraction (*IF*) and suspended fraction (*SF*) are calculated as follows:

$$IF=N_{inhaled}/N_{total} \tag{3a}$$

$$SF=N_{suspended}/N_{total} \tag{3b}$$

Where $N_{inhaled}$ and $N_{suspended}$ are the number of the droplets/droplet nuclei inhaled by the susceptible person and suspended in rooms, respectively. N_{total} is the total number of droplets released from the infected person's mouth and nose. This study investigates a total of 18 investigated cases according to the different location of the index patient, i.e., respectively eight cases when index patient in windward and leeward floors (indoors) and two cases in different site of canyon (outdoors) (Table. 2). Supported by the National Supercomputer Center in Guangzhou, all CFD simulations were finished on Tianhe II supercomputer.

3 Results and discussion

3.1 Flow field and ventilation capability in street canyons and indoors

As depicted in Fig. 6a, there is a clockwise vortex in the street canyon. Vertical movement can be found near the windward side and leeward side of the building wall, and the streamlines are basically parallel to the building wall except in the corner. The normalized velocity at the pedestrian level (Fig. 6b) shows that the largest wind speed (≈1.05 m/s) is appeared in the middle of the canyon (about twice the area near the buildings on both sides of the canyon), and fluctuations are produced in the corner of the first floors of the windward and leeward side buildings. The changing wind speed and direction in the corner will influence the droplet dispersion in outdoors and in the low-level indoor rooms.

Indoor temperature and velocity distribution have been displayed in Fig. 6c-d. It shows that the indoor temperature is higher in the top than in the bottom due to the body thermal plume -- an updraft around the human body. It appears that the 2nd to 7th floors in the leeward building and the 4th to 6th floors in the windward building experience a higher average temperature than other floors, due to the limitation of air change rate between indoor and outdoor. Fig.6d indicate that body thermal plume greatly impacts the indoor airflow. The airflow velocity is smaller than 0.1 m/s in most indoor spaces but about 0.2 m/s above the head. In general, the wind velocity in windward rooms is larger than that in leeward rooms, leading to a higher temperature and weaker ventilation performance in leeward rooms. The airflow pattern of the same side rooms is similar, with the air entering the room from the lower part of the window, then forming a weak vortex between the person and the window. There is a uniform upward flow between the two people, and then the air is discharged from the upper part of the window.

Fig. 6e displays the air change rates per hour for purging flow rate (ACH_{PFR}) in all windward and leeward rooms, which is used to evaluate overall ventilation capacities. For floors with the same height, the ACH_{PFR} in windward is greater than that in leeward, which is consistent with the velocity distribution. For different floors, the near ground floors (1st floor) and top floor (8th floor) have the highest ACH_{PFR} than middle floors (2nd-7th floors) for both windward and leeward buildings of the canyon. In order to make the subsequent analysis more convenient, we divide all rooms into the following three categories according to the indoor ACH_{PFR}. One is the lower part of the street canyon (the 1st floor), where the turbulence fluctuation makes good ventilation (ACH_{PFR}~6.57 h^{-1} and 4.50 h^{-1} respectively in windward and leeward 1st floor); The other is the middle floors of the street canyon (the 2nd-6th floors), where the parallel wind to the window lead to small ACH_{PFR}, with the average ACH_{PFR} of about 3.28 h^{-1} and 1.97 h^{-1} respectively in windward and leeward middle rooms; The last is the high floors (the 7th and 8th floors) which hold better ventilation, with about 5.94 h^{-1} and 4.97 h^{-1} on windward and leeward 8th floors, respectively, due to the high wind speed at the upper corner of the canyon vortex.

3.2 Exposure risk analysis when index patient indoors

Our previous research [11, 27] has found that droplet diffusion characteristics and range are dominated by the interplay of the airflow and ambient temperature. Therefore, we selected three floors (1st, 5th, 8th floors) as a representative for analysis from the aforementioned three types: lower part, middle floors and high floors. The droplet distribution characteristics will be similar in rooms of the same type.

Fig.7 displays the dispersion process of droplets with an initial particle size of 10 μm when the infected person is in windward and leeward side floors, taking 1st, 5th, 8th floors for example. It indicates that the droplets move following the indoor and outdoor airflows because they evaporate rapidly into 3.64 μm nuclei (~0.1 s) in a dry environment of relative humidity RH = 35% which is similar with the finding in our previous studies [11, 27]. We find that most of the droplet nuclei are still suspended in the room where the patient is located, and a small number of them disperse to the street canyon and then enter other rooms. For both windward and leeward, the rising and circulating air flow carries the droplet nuclei to the window and then outdoors. A part of them reenter to the room due to turbulence at the window and fill the whole room over time. The results agree well with Zhang and Li [55] who simulated 48 thermal manikins in a high-speed rail cabin, suggesting that the exhaled droplets tended to follow the upward body thermal plume and could directly enter the upper zone.

Droplets released by the patient on the windward 1st and 8th floors may disperse to the street canyon more quickly than those released on the windward 5th floor. When the patient is on the windward 1st floor, the droplet nuclei escaped from the room will join the fluctuation in the corner of the windward building (Fig. 6(a)), then move up to the height of the 3rd floor. Therefore, when the patient is on the windward 1st floor, the pathogen-laden droplets can spread to windward 2nd and 3rd floors. When the patient is on the windward 8st floor, the droplet nuclei dispersed to the street canyon will re-entry to the lower floor rooms of the same building, which agrees well with Ai et al. [56]. When the infected person is located in leeward rooms, the number of droplet nuclei reentering the rooms is less than that on the windward side rooms. Especially when the patient is on the leeward 8th floor, the releasing droplets will disperse to the urban boundary layer due to the near building upward airflow. Contrary to the case of the patient in windward rooms, the droplet nuclei are more likely to disperse to the urban boundary layer, thereby reducing the number of droplets dragged into the target street canyon.

On one hand, the exposure risk will be greatly increased for the susceptible person staying in the same room with the infected person. Thus, we discuss the circumstance when the susceptible person is in the same room with the infected person and the resulting exposure risk (*IF*) of the susceptible person (Fig.8). From this figure, we can find that the *IF* of the susceptible person in the windward rooms are larger than those in the leeward except rooms on the 2nd and 3rd floors, which is consistent with the wind velocity distribution. It is found that *IF* of the 1st floor (*IF*~4.29 ppm and 1.77 ppm in windward and leeward, respectively) and of the 8th floor (*IF* ~3.03 ppm and 1.77 ppm in windward and leeward, respectively) are smaller than those of other floors. *IF* of floors 4 to 7 are similar (e.g., *IF* in leeward 4th to 7th floors is 3.54 to 6.57ppm). Overall, when a susceptible person is in the same room with the infected person, the most dangerous situation is that they are located on the 6th floor on the windward side and the 2nd and 3rd floors on the leeward side.

On the other hand, the droplets spreading to other rooms will be suspended in the air, leading to the risk of infection to people on other floor or in the canyon, hence there is a need for a further count of the suspended droplet nuclei in each room when the patient is on various floors. *SF* of various rooms when the patient is on different floors have been listed in Table.3. Note that all data in the table are in ppm. The double underlined data are *SF* in the rooms where the infected is located, and the data marked with orange highlight the relatively larger *SF* (i.e., greater than 50 ppm). *SF* in the patient's room is the highest, reaching up to 10^4 ppm, which is around 2-4 orders larger than rooms at other floors without patient. Moreover, the larger wind speed and better ventilation (ACH_{PFR}~6.57 h^{-1} and 4.50 h^{-1} respectively in windward and leeward 1st

floor, and 5.94 h^{-1} and 4.97 h^{-1} in windward and leeward 8th floors) in upper/lower floor carry more droplets entering the canyon, and the exposure risk in these floors is small (e.g., *SF*~1.55×10^4-2.12×10^4 ppm).

From the aforementioned droplet dispersion process, we know that there is an upward movement near the building on windward 1st-3rd floors. Therefore, when the infected is on the windward 1st or 2nd floor, in addition to the floor where the infected person is located, the 2nd and 3rd floors are also the key areas for prevention and measures. The *SF* can reach 572.22 ppm when the infected is on the windward 1st floor. When the infected is on the windward 3rd or 4th floor, there is a small ratio of droplets reentering other floors following the ambient vortexes. It also shows that when the infected is located above the 3rd floor on the windward side, the floor below it will be affected by the airflow, and the floor closed to the source room may have the greatest impact, due to the downward transport induced by the combination of gravity and wind effects [57-58]. When the droplets are released from the leeward floor, the main affected area is the room on the upper floor due to the near building upward airflow induced by the canyon vortex. Generally speaking, when the infected person is in the windward side rooms, the impact range is not only on the floor on its own side, but also spread to the upstream buildings (i.e., leeward side rooms) with the airflow. The average *SF* in the street canyon is 0.81×10^4 ppm, which is more than three times that of when the infected person is in the leeward side rooms (the average is 0.23×10^4 ppm).

3.3 Exposure risk analysis when index patient stays outdoors

It is suggested that staying outdoors may have a much lower infection risk compared with the indoor environment [59]. Nevertheless, an increasing number of cases of infection shows that there is also a risk of infection outdoors [60-61], and it is important to assess the infection risk in outdoor activities.

Fig.9 and Table. 4 illustrate the dispersion process when the infected person is outdoors. In terms of the susceptible person facing to the infected person outdoors, the exposure includes the short spraying transmission (~1m) and the long distance transmission through the entire canyon (~100m). Droplet inhaled here are the total inhaled number by the susceptible person during the calculation period. In general, the number of inhaled droplets is rather small, but large quantities of droplets circulate around, increasing the possibility of inhalation and there are also some differences to some extent in the two outdoor situations. When the infected person is on the leeward corner of the canyon where local urban wind is weak (Fig. 9a), the upward body thermal plume can be clearly found around human, and the relatively small flow in leeward-side corner of the street canyon will result in a larger number of droplets inhaled by the susceptible person (*IF* is 54.8ppm), which is short spraying exposure. When further considering the situation of two people staying in the middle of the canyon (Fig.9b), the parallel and much larger airflow passes between the infected and susceptible persons. In this situation, the *IF* is 7.07 ppm, smaller than that of people in leeward corner, which may be caused by the local wind speed and direction. When the susceptible and infected people all stay outdoors, compared with all staying indoors, the susceptible people are relatively safe in the middle, while they are more dangerous when they are all on the leeward side of the canyon.

The outdoor velocity is much greater than the indoor velocity (e.g., the greatest velocity at the pedestrian level is seven times larger than indoors, Fig.6a-d). Besides, the droplets will join the canyon vortex, resulting in a fast diffusion speed and a wide range of droplets. When the infection source exists in the street canyon, it is surprising that the floors with better natural ventilation have higher indoor droplet concentrations due to more frequent indoor and outdoor air exchange, which will also increase the infection risk of indoor people. Therefore, although the ventilation of the 4^{th}-6^{th} floors is worse than that of other floors, the *SF* (31.06 ppm-68.18 ppm) is much smaller than that of other floors when the infected person is in outdoor environment. Moreover, when the infected person stays in the middle of the canyon, droplets are blown away quickly due to the large wind speed in outdoors, and the number of droplets entering the street-side buildings will be greatly reduced to at least one-fifth of that when in the leeward side of the canyon, leading a little impact on indoor environment.

4 Limitations and future work

From this study, we found the local airflow and ventilation may be important to the exhaled droplet dispersion in outdoor, resulting in a big difference for different sites in street canyon, relative locations between people outdoor and the background dominant wind direction, which is worth studying in the future. Besides, more complicated processes and factors will be taken into account, for instance, more atmospheric conditions of solar radiation and ambient relative humidity/temperature as well as wind speed/directions under various urban shape (e.g. emphasizing high-density urban area with small distance between buildings). Such CFD simulations coupling turbulence and radiation processes will be evaluated and validated by our recent scaled outdoor experiments (H~1m) on urban airflow in street canyons [62-63] and that coupling indoor and outdoor [64].

In particular, it is noted that the ambient humidity should be interrelated to temperature, which is reflected by the setting of the evaporation model in the simulation. Therefore, further efforts will be made on the more practical evaporation model of droplets.

Moreover, as we simplified the breathing to continuously exhaling or inhaling may possibly overestimate the exposure risk, more practical human breathing activities with various droplet initial sizes and velocities should be considered to find out the droplet distribution in the air. Last but not least, more complex and practical droplet composition and breath activity like talking, coughing, speech etc., which related to the number and activity of viruses in the droplet, will be integrated to further evaluate the exposure risk.

5 Conclusions

In this work, a coupling model of the indoor and outdoor environment in a target street canyon with two near-road 8-floor buildings was established to evaluate the potential human-to-human exposure risk in a windward building, a leeward building and street canyon when there is an index patient.

Some meaningful points are concluded as follows:

1)Air change rate (ACH_{PFR}) and wind velocity in windward side rooms is greater than that in leeward side, with best ventilation at the lower floors and top floors (~4.5-6.6 h^{-1}) and worst ventilation at the middle floors (~1.6-5.3 h^{-1}). The exposure risk in 1st and 8th floor is smaller than that in other floors (e.g., *IF* ~ 2-4 ppm in 1st and 8th floor, and 4-11 ppm in 2nd-7th floors).

2)If the infected person is located on different floors in near-road building (indoor), the index patient's room experience the largest *SF* (10^4 ppm), about 2-4 orders greater than that in other rooms at other floors without the index patient.

3)When the infected person is in the street canyon (outdoors), the exposure risk (*IF*) of the face-to-face susceptible person varies among the locations, the higher risk appears when they both are in the leeward corner (~55 ppm), and 7 ppm when they are in the middle of the street.

4)When the infected person stands on the windward 1st and 2nd floors, the people on the windward 2nd and 3rd floors must pay more attention for prevention work. While the infected person is on the floor above the windward 3rd floor, the floors below it will be affected. When the leeward floor is the release source, the main affected area is the room on the upper floors.

Based on the results, it is emphasized that there is high possibility of outdoor human-to-human infection induced by droplet dispersion in weak wind regions of 2D street canyons (e.g. leeward corner), even higher than indoor and should be taken seriously.

Acknowledgments

This work was supported by the National Natural Science Foundation of China (grant numbers 41875015, 42005069, and 42175180); The support from UK GCRF Rapid Response Grant on 'Transmission of SARS-CoV-2 virus in crowded indoor environment', the Innovation Group Project of the Southern Marine Science and Engineering Guangdong Laboratory (Zhuhai) (No. 311020001), Guangdong Province Key Laboratory for Climate Change and Natural Disaster Studies (Grant 2020B1212060025), are also gratefully acknowledged. The CFD simulations were conducted on the Tianhe II supercomputer at the National Supercomputer Center, Guangzhou, P.R. China.

References

[1] N.H. Leung, Transmissibility and transmission of respiratory viruses, Nat. Rev. Microbiol., 19 (2021) 528-545.

[2] WHO, WHO Coronavirus (COVID-19) Dashboard, World Heal. Organ. (2022). https://covid19.who.int/ (accessed October 2, 2022).

[3] J. Hang, Y. Li, R. Jin, The influence of human walking on the flow and airborne transmission in a six-bed isolation room: tracer gas simulation, Build. Environ., 77 (2014) 119-134.

[4] Y. Li, W.H. Ching, H. Qian, P.L. Yuen, W.H. Seto, J.K. Kwan, J. Leung, M. Leung, S.C.T. Yu, An evaluation of the ventilation performance of new SARS isolation wards in nine hospitals in Hong Kong, Indoor Built Environ., 16 (2007) 400-410.

[5] M. Beaussier, E. Vanoli, F. Zadegan, H. Peray, E. Bezian, J. Jilesen, G. Gandveau, J.M. Gayraud, Aerodynamic analysis of hospital ventilation according to seasonal variations. A simulation approach to prevent airborne viral transmission

pathway during Covid-19 pandemic, Environ. Int., 158 (2022)106872.

[6] J. Gupta, C.H. Lin, Q. Chen, Risk assessment of airborne infectious diseases in aircraft cabins, Indoor Air, 22 (2012) 388-395.

[7] Z. Han, G.N. To Sze, S.C. Fu, C.Y.H. Chao, W. Weng, Q. Huang, Effect of human movement on airborne disease transmission in an airplane cabin: study using numerical modeling and quantitative risk analysis, BMC Infect. Dis., 14 (2014) 1-19.

[8] S. Mazumdar, S.B. Poussou, C.H. Lin, S. Isukapalli, M.W. Plesniak, Q. Chen, Impact of scaling and body movement on contaminant transport in airliner cabins, Atmos. Environ., 45 (2011) 6019-6028.

[9] Q. Luo, C. Ou, J. Hang, Z. Luo, H. Yang, X. Yang, X. Zhang, Y. Li, X. Fan, Role of pathogen-laden expiratory droplet dispersion and natural ventilation explaining a COVID-19 outbreak in a coach bus, Build. Environ., 220 (2022) 109160.

[10] C. Ou, S. Hu, K. Luo, H. Yang, J. Hang, P. Cheng, Z. Hai, S. Xiao, H. Qian, S. Xiao, Insufficient ventilation led to a probable long-range airborne transmission of SARS-CoV-2 on two buses, Build. Environ., 207 (2022) 108414.

[11] X. Yang, C. Ou, H. Yang, L. Liu, T. Song, M. Kang, H. Lin, J. Hang, Transmission of pathogen-laden expiratory droplets in a coach bus, J. Hazard. Mater., 397 (2020) 122609.

[12] P. Cheng, W. Chen, S. Xiao, F. Xue, Q. Wang, P.W. Chan, R. You, Z. Lin, J. Niu, Y. Li, Probable cross-corridor transmission of SARS-CoV-2 due to cross airflows and its control, Build. Environ., 218 (2022) 109137.

[13] N. Gao, J. Niu, M. Perino, P. Heiselberg, The airborne transmission of infection between flats in high-rise residential buildings: tracer gas simulation, Build. Environ., 43 (2008) 1805-1817.

[14] Y.C. Tung, S.C. Hu, T.I. Tsai, I.L. Chang, An experimental study on

ventilation efficiency of isolation room, Build. Environ., 44 (2009) 271-279.

[15] J. Gupta, C.H. Lin, Q. Chen, Prediction of spatial and temporal distribution of expiratory droplets in an aircraft cabin, International High Performance Buildings Conference, (2010) 56.

[16] Y. Feng, T. Marchal, T. Sperry, H. Yi, Influence of wind and relative humidity on the social distancing effectiveness to prevent COVID-19 airborne transmission: A numerical study, J. Aerosol. Sci., 147 (2020) 105585.

[17] J. Liu, J. Niu, C.M. Mak, Q. Xia, Detached eddy simulation of pedestrian-level wind and gust around an elevated building, Build. Environ., 125 (2017) 168-179.

[18] Z. Ai, C.M. Mak, A study of interunit dispersion around multistory buildings with single-sided ventilation under different wind directions, Atmos. Environ., 88 (2014) 1-13.

[19] Y. Dai, C.M. Mak, Z. Ai, J. Hang, Evaluation of computational and physical parameters influencing CFD simulations of pollutant dispersion in building arrays, Build. Environ., 137 (2018) 90-107.

[20] K. Zhang, G. Chen, X. Wang, S. Liu, C.M. Mak, Y. Fan, J. Hang, Numerical evaluations of urban design technique to reduce vehicular personal intake fraction in deep street canyons, Sci. Total Environ., 653 (2019) 968-994.

[21] H. Yang, T. Chen, Y. Lin, R. Buccolieri, M. Mattsson, M. Zhang, J. Hang and Q. Wang, Integrated impacts of tree planting and street aspect ratios on CO dispersion and personal exposure in full-scale street canyons, Build. Environ., 169 (2020), 106529.

[22] J. Hang, Z. Xian, D. Wang, C.M. Mak, B. Wang, Y. Fan. The impacts of viaduct settings and street aspect ratios on personal intake fraction in three-dimensional urban-like geometries, Build. Environ., 143 (2018)138-162.

[23] J. Hang, J. Liang, X. Wang, X. Zhang, L. Wu, M. Shao. Investigation of O3–

NOx–VOCs chemistry and pollutant dispersion in street canyons with various aspect ratios by CFD simulations, Build. Environ., 226 (2022) 109667.

[24] R.Ş. Popescu, L. L. Popescu. Assessment of Air Pollution, by the Urban Traffic, in University Campus of Bucharest. J. Environ. Protec. 8 (2017) 884-897

[25] T.C. Bulfone, M. Malekinejad, G.W. Rutherford, N. Razani, Outdoor transmission of SARS-CoV-2 and other respiratory viruses: a systematic review, J. Infect. Dis., 223 (2020) 550-561.

[26] B. Blocken, F. Malizia, T. van Druenen, T. Marchal, Towards aerodynamically equivalent COVID19 1.5 m social distancing for walking and running, preprint, (2020).

[27] X. Yang, H. Yang, C. Ou, Z. Luo, J. Hang, Airborne transmission of pathogen-laden expiratory droplets in open outdoor space, Sci. Total Environ., 773 (2021) 145537.

[28] X. Fan, X. Zhang, A.U. Weerasuriya, J. Hang, L. Zeng, Q. Luo, C.Y. Li, Z. Chen, Numerical investigation of the effects of environmental conditions, droplet size, and social distancing on droplet transmission in a street canyon, Build. Environ., 221 (2022) 109261.

[29] L. Bourouiba, Turbulent gas clouds and respiratory pathogen emissions: Potential implications for reducing transmission of COVID-19, JAMA, 323 (2020) 1837-1838.

[30] S. Mei, C. Yuan, Urban buoyancy-driven air flow and modelling method: a critical review, Build. Environ. , 210 (2021) 108708.

[31] L.L. Popescu, R.S. Popescu, T. Catalina, Indoor particle’s pollution in Bucharest, Romania. Toxics, 10 (2022) 120757.

[32] L.C. Marr, J.W. Tang, J. Van Mullekom, S.S. Lakdawala, Mechanistic insights into the effect of humidity on airborne influenza virus survival, transmission and incidence, J. R. Soc. Interface, 16 (2019) 20180298.

[33]J. Wei, Y. Li, Enhanced spread of expiratory droplets by turbulence in a cough jet, Build. Environ., 93 (2015) 86-96.

[34]C. Gao, Y. Li, J. Wei, S. Cotton, M. Hamilton, L. Wang, B.J. Cowling, Multi-route respiratory infection: when a transmission route may dominate, Sci. Total Environ., 752 (2021) 141856.

[35]F. Liu, Z. Luo, Y. Li, X. Zheng, C. Zhang, H. Qian, Revisiting physical distancing threshold in indoor environment using infection-risk-based modeling, Environ. Int., 153 (2021) 106542.

[36]B. Blocken, Computational Fluid Dynamics for urban physics: importance, scales, possibilities, limitations and ten tips and tricks towards accurate and reliable simulations, Build. Environ., 91 (2015) 219-245.

[37]R.N. Meroney, Ten questions concerning hybrid computational/physical model simulation of wind flow in the built environment, Build. Environ., 96 (2016) 12-21.

[38]X. Li, C.H. Liu, D.Y. Leung, Numerical investigation of pollutant transport characteristics inside deep urban street canyons, Atmos. Environ., 43 (2009) 2410-2418.

[39]R.N. Meroney, M. Pavageau, S. Rafailidis, M. Schatzmann, Study of line source characteristics for 2-D physical modelling of pollutant dispersion in street canyons, J. Wind Eng. Ind. Aerodyn., 62 (1996) 37-56.

[40]X. Xie, Z. Huang, J. Wang, The impact of urban street layout on local atmospheric environment, Build. Environ., 41 (2006) 1352-1363.

[41]X. Yang, Y. Zhang, J. Hang, Y. Lin, M. Mattsson, M. Sandberg, M. Zhang, K. Wang, Integrated assessment of indoor and outdoor ventilation in street canyons with naturally-ventilated buildings by various ventilation indexes, Build. Environ., 169 (2020) 106528.

[42]B. Blocken, LES over RANS in building simulation for outdoor and indoor applications: a foregone conclusion? Build. Simul., 11 (2018) 821-870.

[43]P. Mishra, K.R. Aharwal, A review on selection of turbulence model for CFD analysis of air flow within a cold storage, in: IOP conference series: Materials science and engineering, IOP Publishing, 2018, pp. 012145.

[44]T. Van Hooff, B. Blocken, On the effect of wind direction and urban surroundings on natural ventilation of a large semi-enclosed stadium, Comput. Fluids, 39 (2010) 1146-1155.

[45]J.O. Cheung, C.H. Liu, CFD simulations of natural ventilation behaviour in high-rise buildings in regular and staggered arrangements at various spacings, Energy Build., 43 (2011) 1149-1158.

[46]R. Jin, J. Hang, S. Liu, J. Wei, Y. Liu, J. Xie, M. Sandberg, Numerical investigation of wind-driven natural ventilation performance in a multi-storey hospital by coupling indoor and outdoor airflow, Indoor Built. Environ., 25 (2016) 1226-1247.

[47]H. Qian, Y. Li, Removal of exhaled particles by ventilation and deposition in a multibed airborne infection isolation room, Indoor Air, 20 (2010) 284-297.

[48]C.H. Liu, C.T. Ng, C.C. Wong, A theory of ventilation estimate over hypothetical urban areas, J. Hazard. Mater., 296 (2015) 9-16.

[49]C. Sha, X. Wang, Y. Lin, Y. Fan, X. Chen, J. Hang, The impact of urban open space and 'lift-up' building design on building intake fraction and daily pollutant exposure in idealized urban models, Sci. Total Environ., 633 (2018) 1314-1328.

[50]L. Liu, J. Wei, Y. Li, A. Ooi, Evaporation and dispersion of respiratory droplets from coughing, Indoor Air, 27 (2017) 179-190.

[51]M. Brown, R.E. Lawson, D.S. DeCroix, R.L. Lee, Comparison of centerline velocity measurements obtained around 2D and 3D building arrays in a wind tunnel,

Los Alamos: National laboratory (2001) Report LA-UR-01-4138.

[52]Y. Ji, H. Qian, J. Ye, X. Zheng. The impact of ambient humidity on the evaporation and dispersion of exhaled breathing droplets: A numerical investigation. J. Aerosol Sci. 115 (2018) 164-172.

[53]R. Ramponi, B. Blocken, CFD simulation of cross-ventilation for a generic isolated building: impact of computational parameters, Build. Environ., 53 (2012) 34-48.

[54]J.L. Potter, L.W. Matthews, J. Lemm, S. Spector, Human pulmonary secretions in health and disease. Annals of the New York Academy of Sciences. 106(1963) 692-697.

[55]L. Zhang, Y. Li, Dispersion of coughed droplets in a fully-occupied high-speed rail cabin, Build. Environ., 47 (2012) 58-66.

[56]Z. Ai, C.M. Mak, D. Cui, On-site measurements of ventilation performance and indoor air quality in naturally ventilated high-rise residential buildings in Hong Kong, Indoor Built Environ., 24 (2015) 214-224.

[57]C. Chen, B. Zhao, Some questions on dispersion of human exhaled droplets in ventilation room: answers from numerical investigation. Indoor Air, 20(2010) 95-111.

[58]B. Zhao, Y. Zhang, X. Li, X. Yang, D. Huang, Comparison of indoor aerosol particle concentration and deposition in different ventilated rooms by numerical method. Build. Environ., 39(2004) 1-8.

[59]Y. Dai, C.M. Mak, Z. Ai, Flow and dispersion in coupled outdoor and indoor environments: Issue of Reynolds number independence, Build. Environ., 150 (2019) 119-134.

[60]S.A. Clouston, O. Morozova, J.R. Meliker, A wind speed threshold for

increased outdoor transmission of coronavirus: an ecological study, BMC Infect. Dis., 21 (2021) 1-9.

[61] X. Zhang, Z. Ji, Y. Yue, H. Liu, J. Wang, Infection risk assessment of COVID-19 through aerosol transmission: a case study of South China seafood market, Environ. Sci. Technol., 55 (2021) 4123-4133.

[62] G. Chen, X. Yang, H. Yang, J. Hang, Y. Lin, X. Wang, Q. Wang, Y. Liu, The influence of aspect ratios and solar heating on flow and ventilation in 2D street canyons by scaled outdoor experiments, Build. Environ., 185 (2020) 107159.

[63] J. Hang and G. Chen, Experimental study of urban microclimate on scaled street canyons with various aspect ratio, Urban Clim., 46 (2022), 101299.

[64] Y. Dai, C.M. Mak, J. Hang, F. Zhang, H. Ling. Scaled outdoor experimental analysis of ventilation and interunit dispersion with wind and buoyancy effects in street canyons. Energy Build. 255 (2022) 111688.

Appendix: Validation of the buoyancy effect

Before cases investigation, a former simulation of buoyancy effect, ventilation mode in a real inpatient ward (Yin et al, 2009) have been conducted to evaluate the accuracy of CFD simulation (Fig. S1a). The isolation room equipped with displace ventilation supply rate of 114 cubic feet per minute (CFM), 19.5℃ of temperature, and the 36CFM and 78CFM of rates in the bathroom and main exhausts respectively. Patients, visitors, TV and equipment generate 106W, 110W, 24W and 36W heat respectively. The mesh was generated with the maximum grid size of 5cm, totaling tetrahedral cells of 1.8 million. The measurement locations are marked in Fig. S1b.

Velocity, temperature of the experiment and simulation results are compared. Fig. S2 displays the normalized velocity (u/U, U=0.14m/s is the supply air velocity) and the normalized temperature ($\Theta=(T-T_i)/(T_e-T_i)$, T_i and T_e are the temperature respectively at inlet and main exhaust) along the normalized height (z/H, H=2.7m is the height of the inpatient ward) in Pole 4 and Pole 5 for example. From the results, it is found that the CFD have a good performance in predicting the velocity and temperature field in this isolation chamber. The Pearson correlations of velocity and temperature are >0.71 and >0.94 respectively. The velocity and temperature are slightly overestimate while they still show the good agreement of the experiment data. Therefore, the above comparison proves the CFD simulation is an effective tool in simulating the flow field including the buoyancy effect.

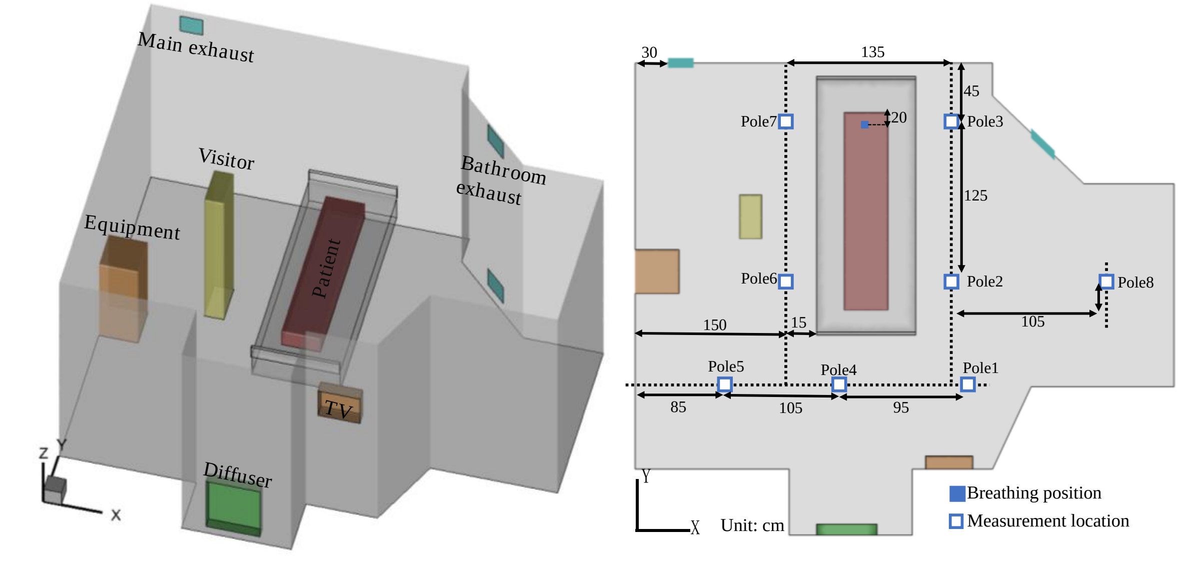

(a) (b)

Fig. S1 (a) Overview of the isolation room, (b) measurement location

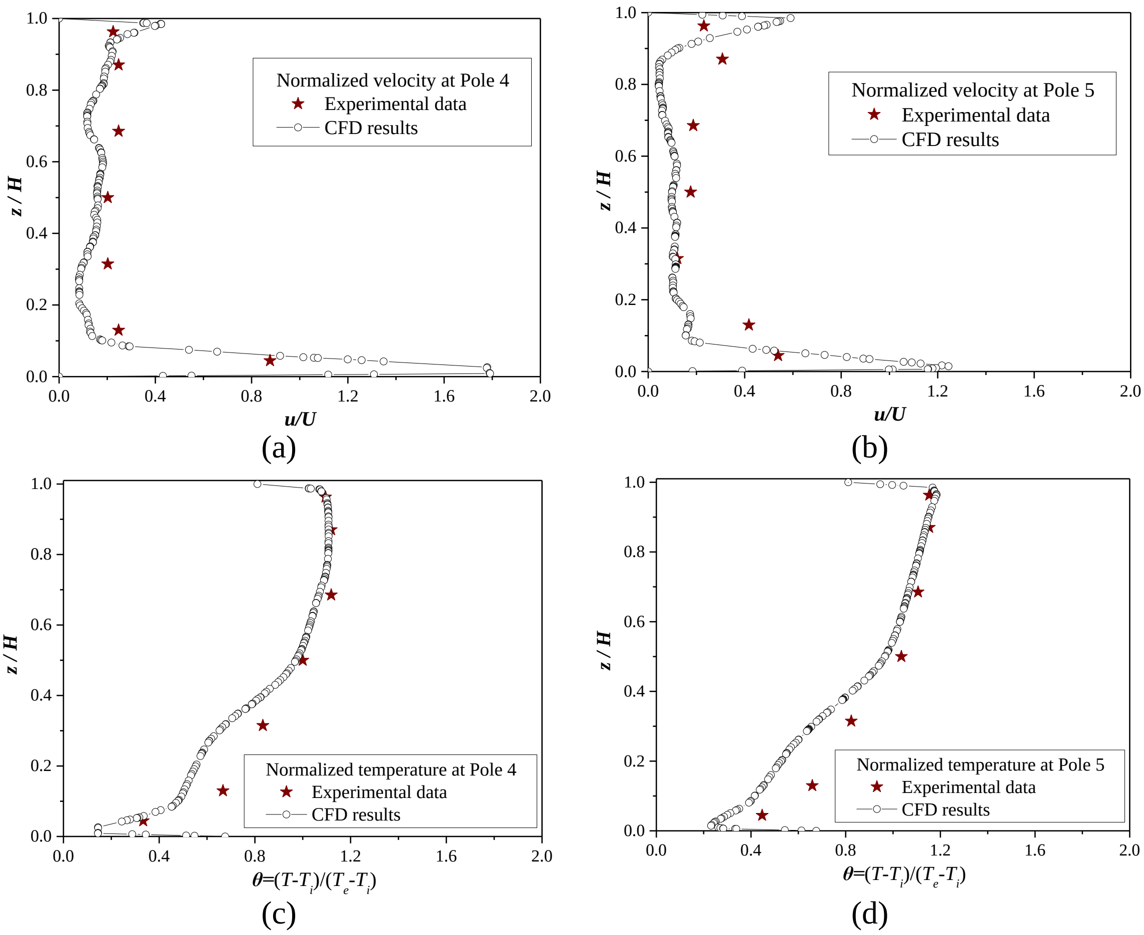

Fig. S2 Comparison of (a)(b)velocity and (c)(d)temperature distribution between CFD and measurement

Yin, Y., Xu, W., Gupta, J., Guity, A., Marmion, P., Manning, A., Gulick, B., Zhang, X., Chen, Q. 2009. Experimental study on displacement and mixing ventilation systems for a patient ward. HVAC and R Research. 15(6), 1175-1191.

Table. 1 Boundary condition setups in CFD simulations.

Boundary name	Boundary condition of airflow	Boundary condition of droplet
Domain inlet	**Velocity inlet**, the vertical velocity obeys the exponential profile and temperature is 300℃, and turbulent intensity is 5 %.	**Escape** (trajectory calculations are terminated here)
Domain outlet	**Outflow**	**Escape** (trajectory calculations are terminated here)
Domain roof, laterals	**Symmetry**	**Escape** (trajectory calculations are terminated here)
Domain floor, building surfaces	**No slip wall**	**Trap** (trajectory calculations are terminated here)
Mouth of infected patient	**Mass-flow-inlet**, mass flow rate is 1.225×10^{-4} kg/s (in a direction perpendicular to human mouth), temperature is 308℃.	**Escape** (trajectory calculations are terminated here)
Mouth of susceptible person	**Mass-flow-outlet**, mass flow rate is 1.225×10^{-4} kg/s (in a direction perpendicular to human mouth), temperature is 308℃.	**Escape** (trajectory calculations are terminated here)
Other body surfaces	**No slip wall**, heat flux is 58 W/m^2 for each person.	**Trap** (trajectory calculations are terminated here)

Table. 2 Parameters and setups for 18 simulations.

Case	Infected patient location
Case 1-8	**Indoors,** 1st floor to 8th floor in windward-side building
Case 9-16	**Indoors,** 1st floor to 8th floor in leeward-side building
Case 17	**Outdoors,** leeward side corner of canyon
Case 18	**Outdoors,** middle of canyon

Table. 3 Suspended fraction (*SF*) in each room when patient in different floors. Unit: ppm

		Patient in indoor different floor																Patient in outdoor	
Floor No.		Windward								Leeward								leeward	middle
		1st	2nd	3rd	4th	5th	6th	7th	8th	1st	2nd	3rd	4th	5th	6th	7th	8th		
Windward rooms	1st	1.55×10^4	2.53	1.26	0.51	1.01	2.02	2.78	1.77	0.51	0.51	0.00	0.00	0.25	0.00	0.51	0.00	44.19	7.07
	2nd	252.78	2.31×10^4	1.77	2.02	0.76	1.01	1.77	0.51	0.25	1.01	0.00	0.25	0.00	0.25	0.25	0.51	34.09	6.31
	3rd	572.22	195.45	2.07×10^4	7.58	6.57	4.55	7.83	2.27	0.51	1.26	0.00	1.01	0.25	0.00	0.25	1.01	79.80	18.18
	4th	1.77	1.01	1.52	2.68×10^4	152.78	75.51	47.22	12.37	1.26	2.27	0.76	0.76	0.00	0.51	1.26	0.25	53.54	9.60
	5th	3.03	0.00	1.01	0.76	2.74×10^4	145.20	64.65	15.15	1.77	0.76	0.51	0.25	0.51	0.00	1.26	1.01	52.78	9.85
	6th	2.27	1.01	2.02	1.52	0.76	2.77×10^4	182.58	27.27	2.02	0.25	0.00	0.00	0.00	0.00	1.77	0.76	68.18	11.62
	7th	1.77	1.01	2.78	2.27	2.27	1.77	2.70×10^4	86.87	3.03	1.26	0.76	2.02	0.51	1.26	2.78	2.53	118.18	16.16
	8th	3.54	1.77	2.27	5.56	2.53	2.53	2.53	1.81×10^4	2.53	2.27	1.52	0.76	0.51	1.01	2.53	2.53	157.07	21.46
	average	\	\	\	\	\	\	\	\	1.48	1.20	0.44	0.63	0.25	0.38	0.33	1.07	75.98	12.53
Target canyon ($\times10^4$)		1.26	0.47	0.71	0.77	0.69	0.81	1.17	0.61	0.57	0.31	0.15	0.15	0.09	0.07	0.26	0.27	21.4	4.20
		Average：0.81								Average：0.23								\	\
Leeward rooms	1st	9.85	6.82	6.31	7.07	4.80	9.09	6.57	2.27	1.78×10^4	0.76	0.25	0.00	0.76	0.51	0.51	1.01	898.23	33.59
	2nd	7.07	3.54	4.80	4.55	4.29	3.54	4.80	4.04	57.83	2.24×10^4	0.51	0.76	0.00	0.51	1.26	0.25	318.69	11.62
	3rd	3.03	2.27	3.03	3.28	0.51	2.02	2.53	1.26	0.51	195.45	2.57×10^4	0.25	0.00	0.00	0.76	0.25	109.85	12.37
	4th	3.03	0.76	1.26	1.01	1.26	2.27	2.02	0.51	1.52	10.35	97.98	2.24×10^4	0.00	0.00	0.25	0.51	34.60	7.32
	5th	3.03	0.25	0.76	0.25	0.51	0.76	1.01	0.51	0.51	4.04	19.95	54.80	2.14×10^4	0.00	0.00	0.51	31.06	7.07
	6th	1.77	0.00	1.26	0.76	0.51	0.00	0.00	0.25	1.26	2.53	9.85	25.76	34.09	2.52×10^4	0.00	0.00	38.64	7.07
	7th	2.02	1.52	2.27	1.26	1.52	3.03	2.27	0.51	2.27	4.29	10.86	17.42	28.54	72.22	2.43×10^4	0.25	78.79	18.69

	8th	7.58	1.77	2.78	3.79	2.27	5.05	4.80	2.78	1.77	0.76	0.51	1.26	1.01	1.01	10.10	2.12×10^4	97.98	15.15
	average	4.67	2.11	2.81	2.75	1.96	3.22	3.00	1.52	\	\	\	\	\	\	\	\	200.98	14.11

Table 4 *IF* of the susceptible person when two people in outdoors.

Exposure index	Site L (Leeward side of canyon)	Site M (Middle of canyon)
***IF* (inhaled fraction)**	54.8ppm	7.07ppm

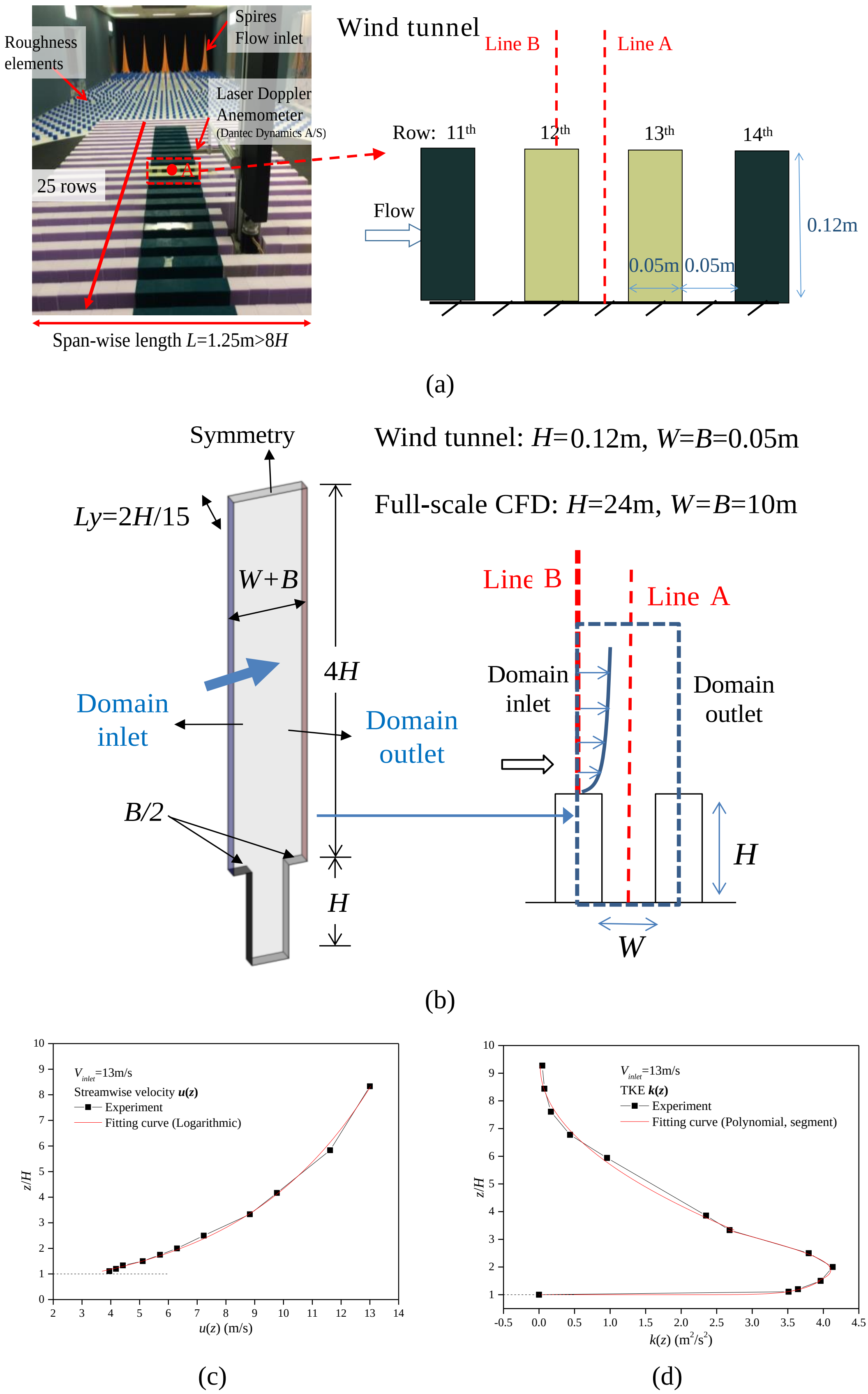

Fig. 1 Validation of urban ventilation. (a) Overview of experiment placement, (b) Full scale model in CFD simulation. Domain inlet boundary condition of (c) stream-wise velocity and (d) turbulence kinetic energy.

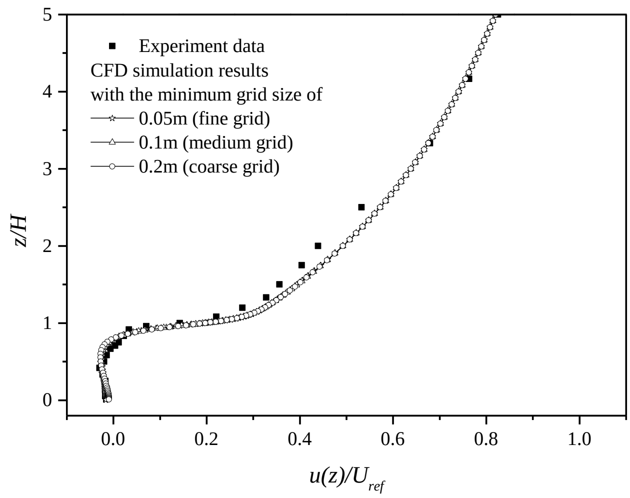

Fig. 2 Comparison of experimental data and CFD simulation results.

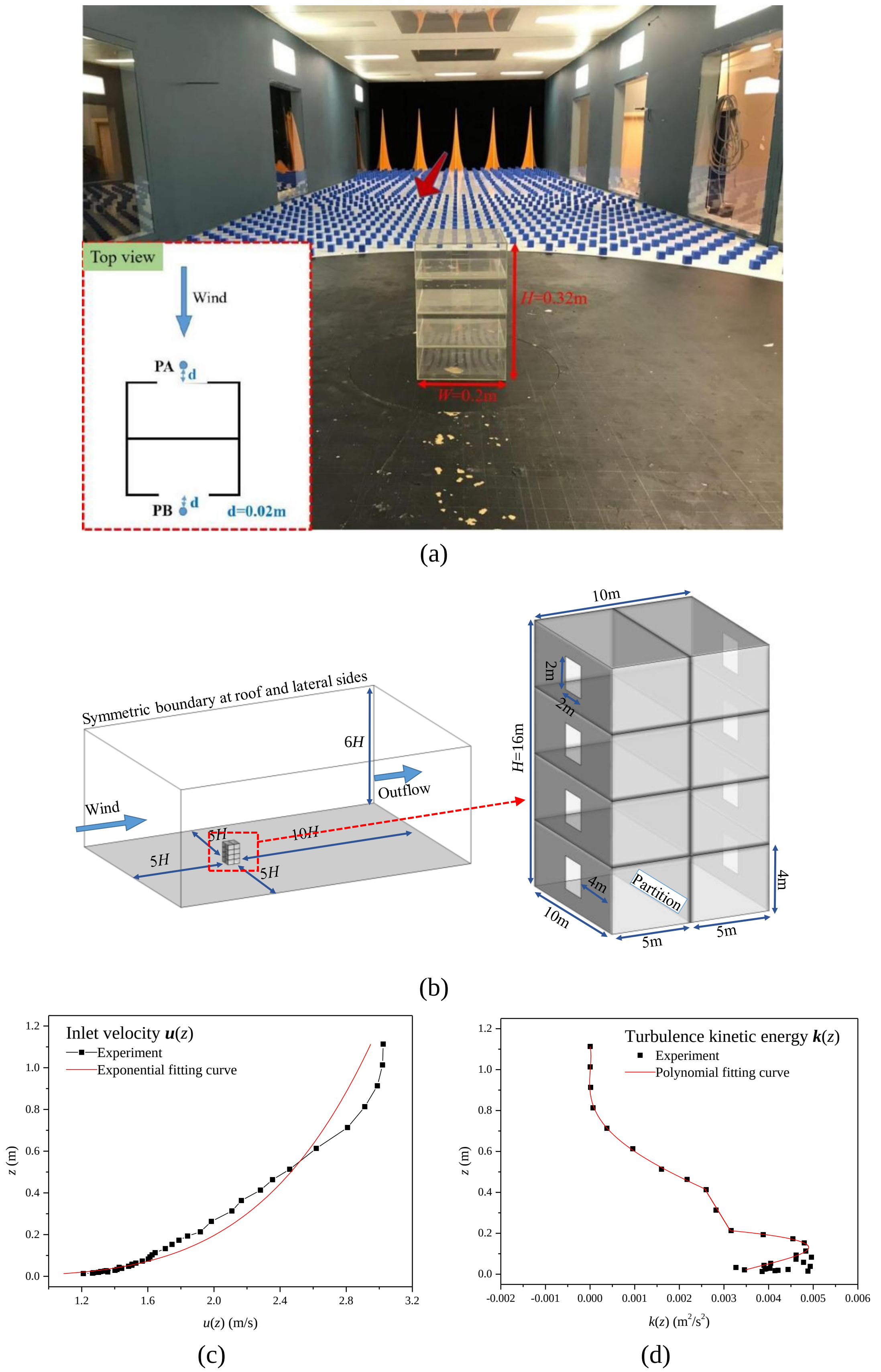

Fig. 3 Validation of indoor and outdoor ventilation. (a) Overview of experiment placement, (b) Full scale model in CFD simulation. Domain inlet boundary condition of (c) stream-wise velocity and (d) turbulence kinetic energy.

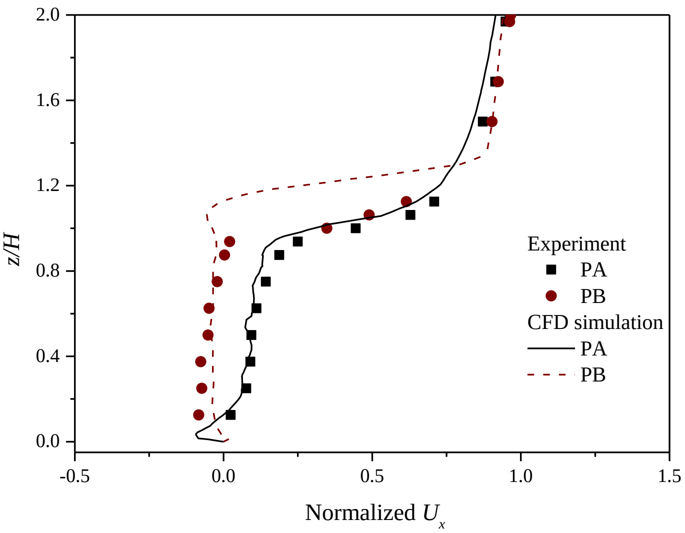

(a)

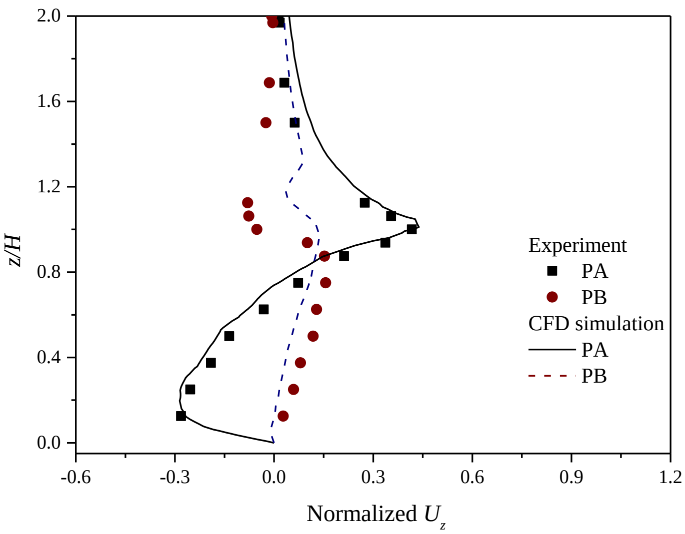

(b)

Fig. 4 Results of experiment data comparing to CFD simulation results. (a) Normalized U_x, (b) Normalized U_z

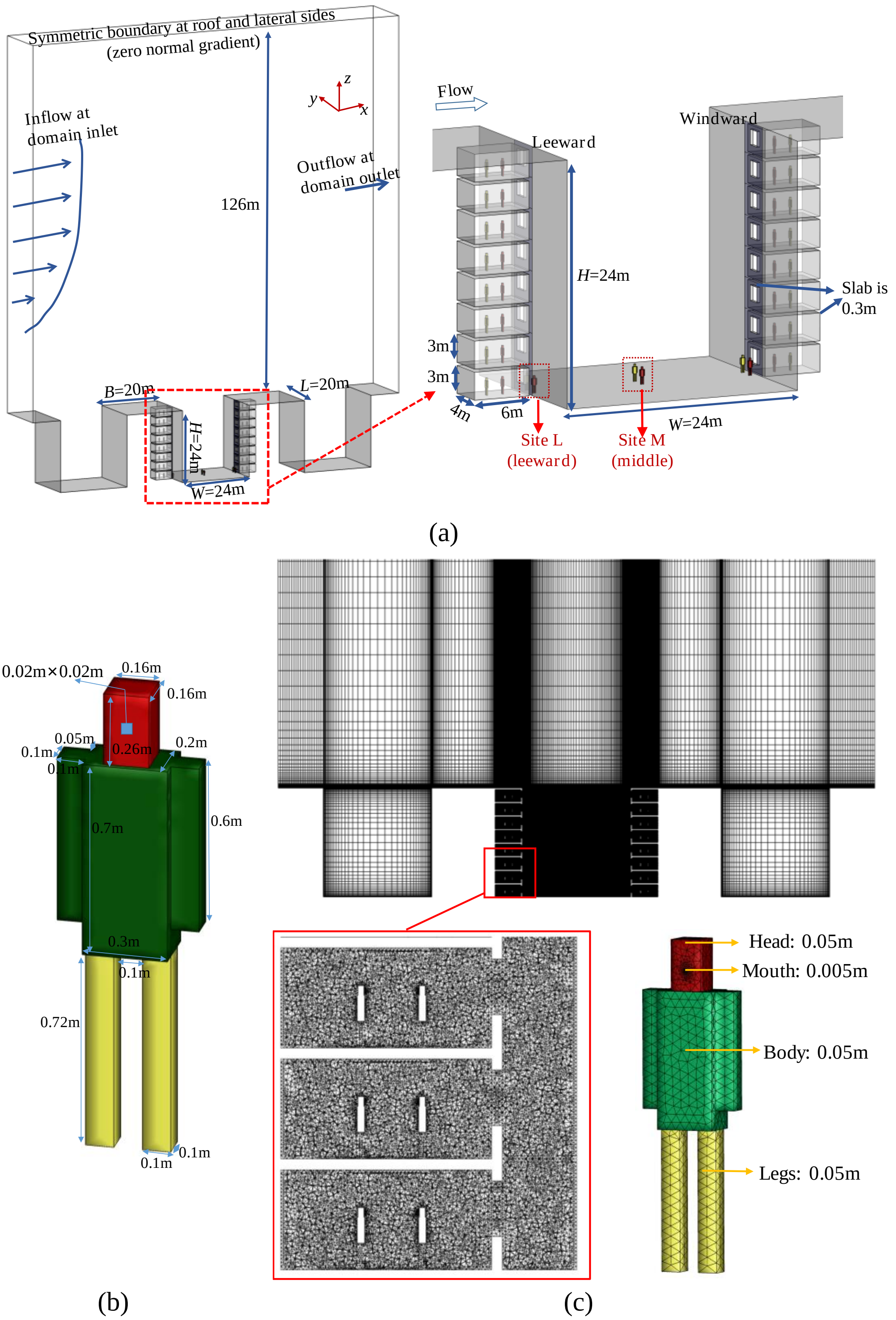

Fig. 5 (a) Urban street canyon in CFD simulation, (b) Detailed information of human model, (c) Grid arrangement on central plane and manikin surface.

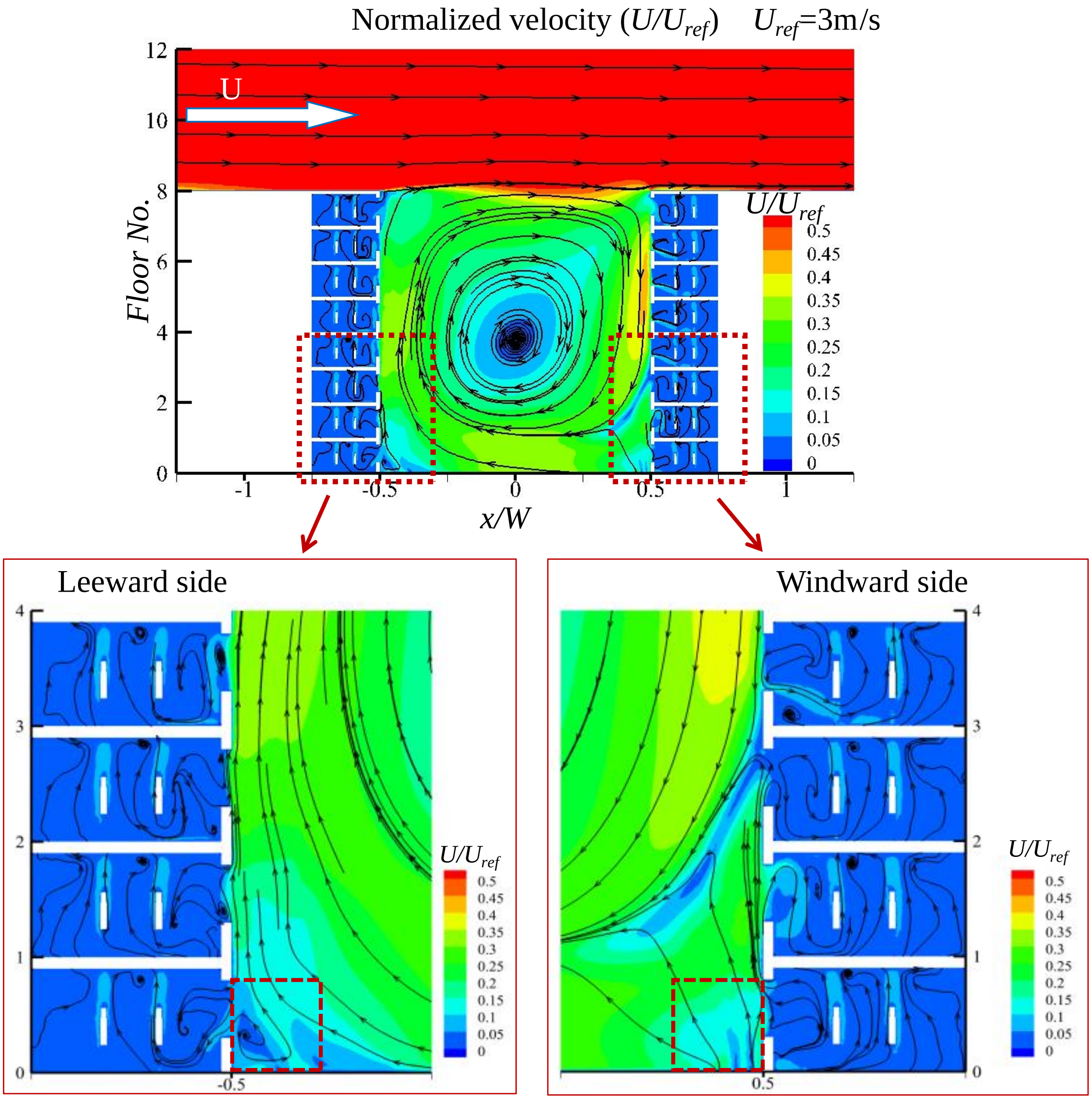

Normalized velocity (U/U_{ref}) U_{ref}=3m/s
U
Floor No.
x/W
U/U_{ref}
0.5
0.45
0.4
0.35
0.3
0.25
0.2
0.15
0.1
0.05
0
Leeward side
Windward side

(a)

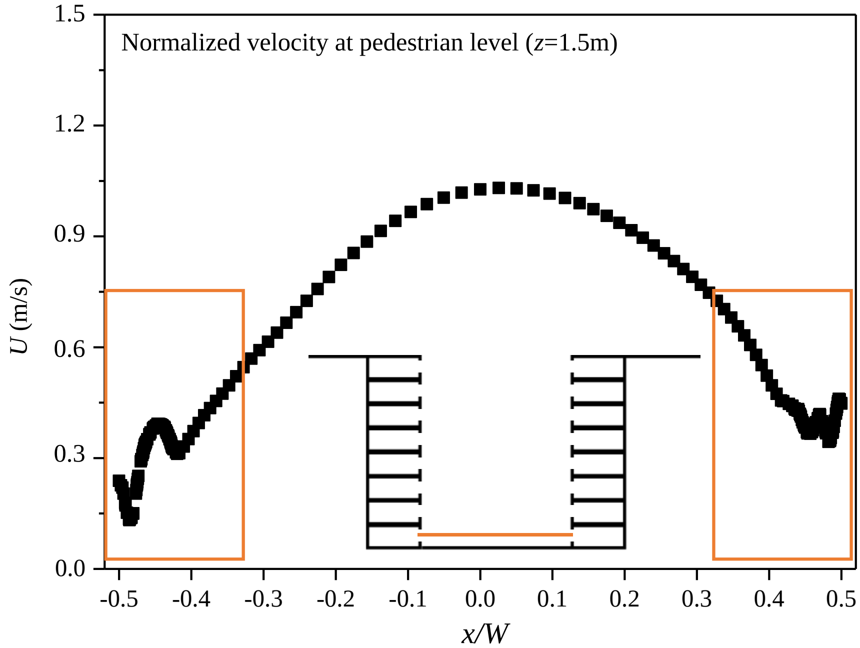

Normalized velocity at pedestrian level (z=1.5m)
U (m/s)
x/W
1.5
1.2
0.9
0.6
0.3
0.0
-0.5
-0.4
-0.3
-0.2
-0.1
0.0
0.1
0.2
0.3
0.4
0.5

(b)

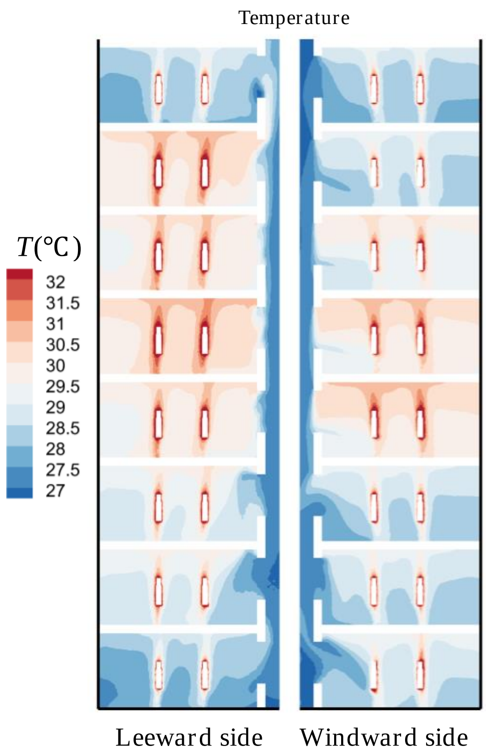

Temperature
T(℃)
32
31.5
31
30.5
30
29.5
29
28.5
28
27.5
27
Leeward side
Windward side

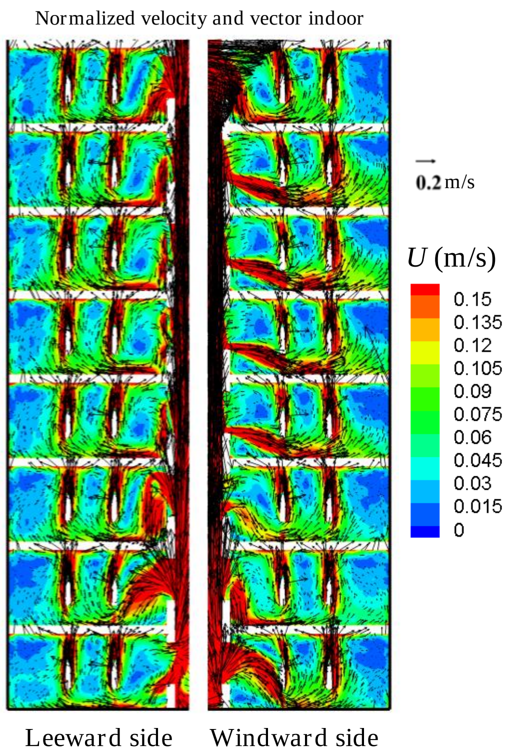

Normalized velocity and vector indoor
0.2 m/s
U (m/s)
0.15
0.135
0.12
0.105
0.09
0.075
0.06
0.045
0.03
0.015
0
Leeward side
Windward side

(c) (d)

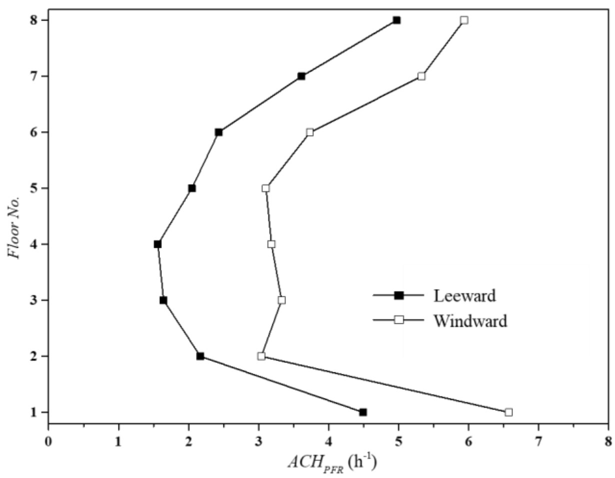

(e)

Fig. 6 (a) Flow field distribution in canyon, (b) Horizontal velocity profile at pedestrian breathing height z =1.5 m, (c) Indoor temperature distribution, (d) Indoor velocity vector superimposed standardized velocity cloud map, (e) Indoor ACH_{PFR}.

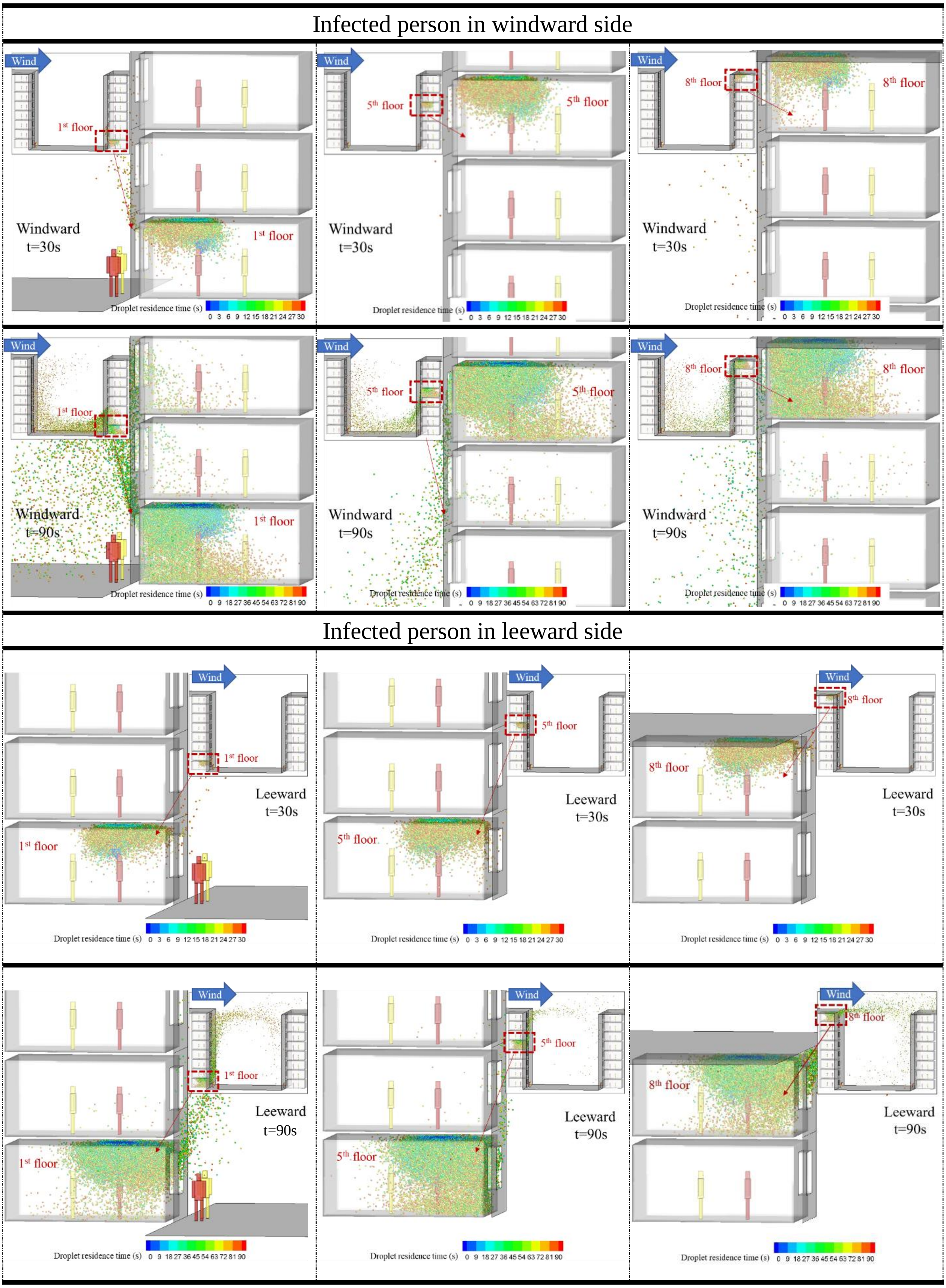

Fig. 7 Dispersion process of droplets with an initial particle size of 10 μm when infected person in windward side and leeward side floors (t = 30 s, 90 s), taking 1st, 5th, 8th as examples.

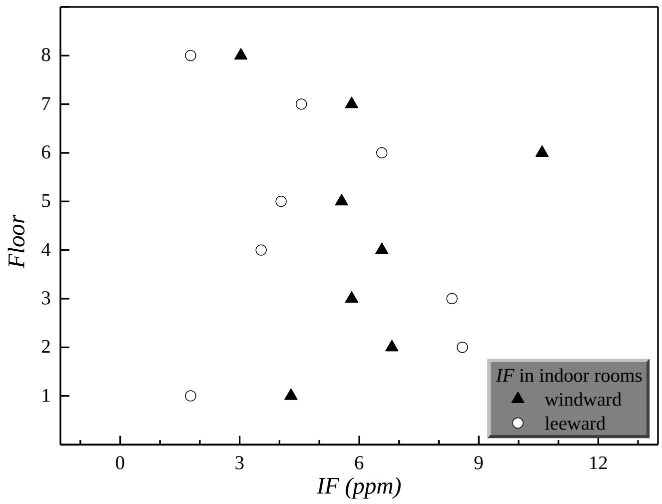

Fig. 8 Inhaled fraction (*IF*) of susceptible person who stay in the same room with the infected person.

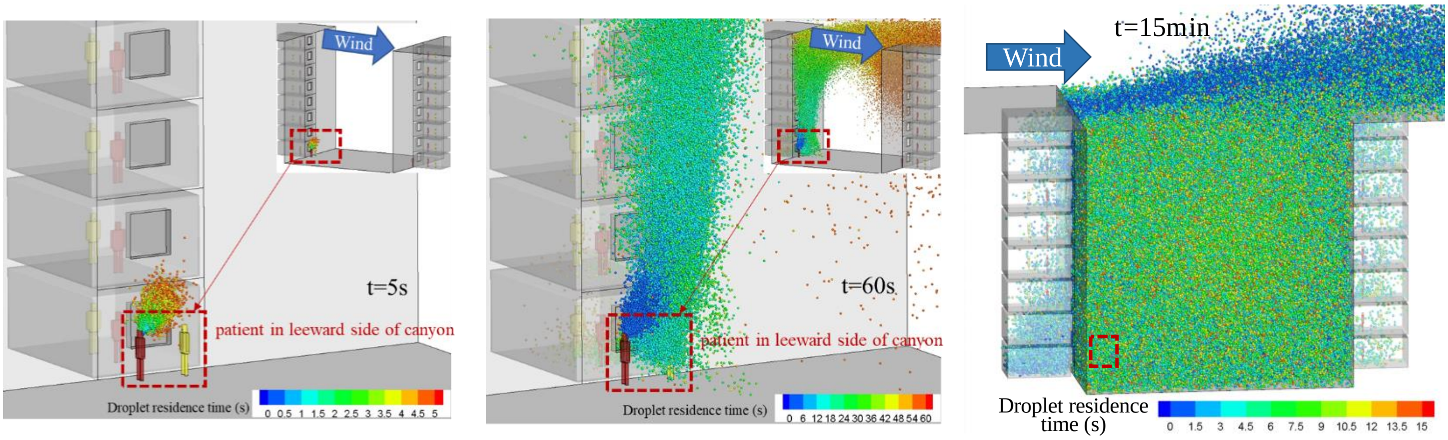

(a)

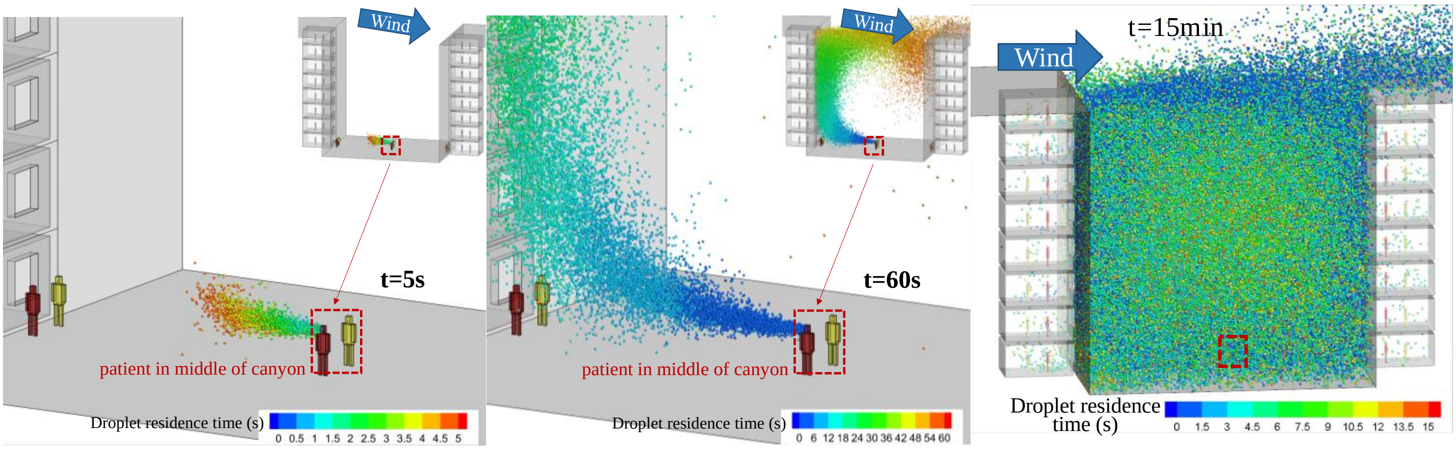

(b)

Figure. 9 Dispersion process (t = 5 s, 60 s, 15 min) when patient in (a) leeward side of canyon, (b) middle of canyon